Reprinted from Applied Optics, Vol. 23, page 2594, August 1, 1984
Copyright © 1984 by the Optical Society of America and reprinted by permission of the copyright owner.

Submillimeter high-resolution FT spectrometer for atmospheric studies

Bruno Carli, Francesco Mencaraglia, and Alberto Bonetti

The rationale, design, and performance of a high-resolution Fourier transform spectrometer are discussed. The instrument was employed in the measurement of stratospheric emission in the 7–90-cm^{-1} spectral interval with a 0.0033-cm^{-1} resolution (unapodized) from a balloon-borne platform at ~40-km altitude.

I. Introduction

High instrumental efficiency can be achieved in the submillimeter spectral region with a two-beam interferometer which uses a free-standing-wire polarizer as a beam splitter (polarizing interferometer[1]). The high efficiency of the polarizing interferometer has been exploited in the spectral analysis of weak sources[2,3] and in accurate radiometric measurements.[4,5] An obvious further application is high-resolution spectroscopy such as that required by atmospheric physics for concentration measurements of trace constituents.

A preliminary test of this application was made in 1975 with an aircraft-borne instrument in the 5–40-cm^{-1} range at a nominal 0.01-cm^{-1} resolution, unapodized.[6] The significance of the 1975 measurements was limited by the pressure broadening of atmospheric lines at aircraft altitude, and it was not possible at the time to make any positive assignment of new lines to minor atmospheric constituents. Nevertheless, the good quality of the spectra suggested that many minor atmospheric constituents could be detected in the stratosphere with an instrument with sufficiently high resolution operating from spacecraft or a balloon platform.[7]

An interferometer optimized to the above purpose has been built and successfully flown at balloon altitude[8–10]: the present paper contains a detailed discussion of its design and characteristics. Instruments devoted to the measurement of atmospheric spectra in the submillimetric region are described in Refs. 11–18.

In Sec. II we discuss the requirements of resolution and instrumental efficiency which have led to the choice of the dimensions of the instrument. The instrument and its major characteristics are described in Sec. III. Section IV contains a discussion of the options adopted in the signal sampling to optimize the efficiency of the instrument. Specific problems such as position control of the moving mirror, choice of the detector, and data analysis are discussed in Secs. V, VI, and VII, respectively. Final remarks on the performance of the instrument are found in Sec. VIII.

II. Design Criteria

In a Fourier transform spectrometer, as long as the light grasp can be kept constant, the SNR of a nonresolved line is independent of the resolution. It is, therefore, advantageous to use a resolution of the order of the halfwidth of the spectral features: this corresponds to a rather high resolution in the case of stratospheric submillimeter spectra, where the single spectral features have a linewidth ranging from 10^{-2} to 10^{-4} cm^{-1} depending on the pressure.

The ultimate choice in the design of the instrument is, in fact, dictated by mechanical constraints. In the present case we compromise on an unapodized resolution of 3.3×10^{-3} cm^{-1} corresponding to a maximum path difference of 150 cm and a mirror movement of 75 cm.

The resolution $\Delta\sigma$ is subject to the Jacquinot condition[19]

$$\Delta\sigma \geq \Omega\sigma/2\pi, \tag{1}$$

where Ω is the solid angle, and σ is the wave number. To keep the $\Delta\sigma = 3.3 \times 10^{-3}$-$cm^{-1}$ resolution up to a nominal $\sigma_{max} = 100$ cm^{-1}, Ω should not be larger than 2×10^{-4} sr.

On the other hand, the signal is proportional to the light grasp $A\Omega$ of the instrument (where A is the cross section of the beam), which should be maximized and possibly made equal to the light grasp $a\omega$ of the detector.

A. Bonetti is with Universita degli Studi di Firenze, Istituto di Fisica Superiore, via S. Marta 3, 50139 Firenze, Italy; the other authors are with Istituto di Ricerca Onde Elettromagnetiche del CNR, via Panciatichi 64, 50127 Firenze, Italy.

Received 2 February 1984.
0003-6935/84/152594-10$02.00/0.
© 1984 Optical Society of America

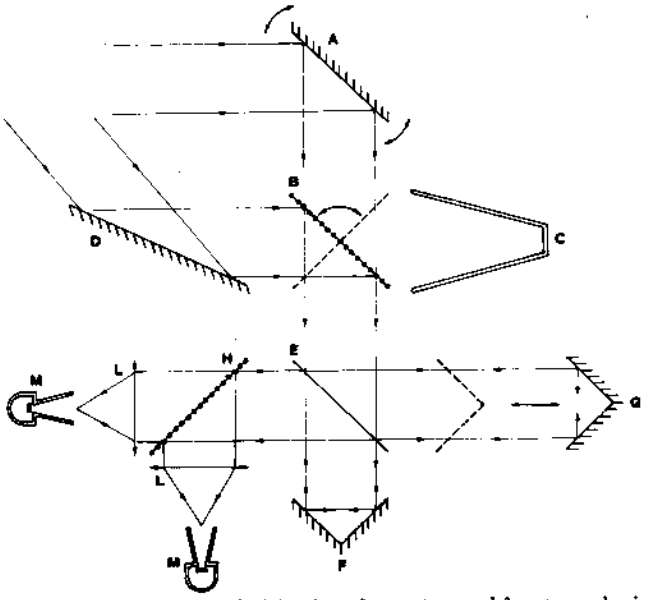

Fig. 1. Layout of the polarizing interferometer used for atmospheric studies: A, mirror for scan of the atmospheric limb; B, input polarizer; C, blackbody source; D, mirror for measurement of zenithal emission; E, polarizing beam splitter; F, fixed roof mirror; G, moving roof mirror; H, output polarizer; L, condensing optics; M, detector.

In the case of submillimetric detectors, $a\omega$ is usually of the order of 0.2 cm^2 sr. This requirement would lead to

$$A = \sqrt{a\omega/\Omega} \simeq 1 \cdot 10^3 \text{ cm}^2 \quad (2)$$

and an optics diameter d equal to

$$d = 4A/\pi \simeq 36 \text{ cm}. \quad (3)$$

This size cannot be achieved because of the present maximum dimensions of good quality free-standing polarizers. The polarizers we have chosen (specially made at the National Physical Laboratory[20]), despite their relatively large dimensions (20-cm diam), allow a beam section not larger than ~12-cm diam when used as a beam splitter at 45°. Again, the mechanical constraints dictated the ultimate choice.

The use of a relatively small beam section imposes a compromise between the two requirements of resolution and light grasp. The solid angle of the instrument, which is defined by the detector aperture, can be varied to optimize either the resolving power at the expense of SNR or vice versa.

The measurements referred to in this paper have been obtained with a solid angle of $\Omega = 5.4 \times 10^{-4}$ sr corresponding to a maximum resolving power of 1.2×10^4.

III. General Characteristics of the Instrument

A. Instrument Layout

The instrument layout is shown in Fig. 1. The atmospheric signal is acquired by mirror A, which can point the atmosphere at different presettable zenithal angles located near the atmospheric limb (emission limb-scan measurements).

The input polarizer B transmits in a polarization plane parallel to its principal axis a linearly polarized component of the atmospheric signal from A and reflects in the perpendicular plane a component of the reference signal entering from the second input port C (or D).

The polarizing beam splitter E has its principal axis at 45° to that of B. So both linearly polarized beams from the input polarizer are split into two equal amplitude beams; one transmitted to the fixed mirror F, the other reflected to the moving mirror G.

F and G are 90° roof mirrors which overturn the reflected image around an axis parallel to the roof edge without introducing an appreciable dichroic effect (in the case of far-infrared radiation). Thus if the roof edges are at a 45° angle to the principal axis of the beam splitter, both the images and the polarization planes of the beams emerging from the beam splitter are rotated by 90° by the reflection on F and G. When reaching back the beam splitter, one of the two beams is reflected and the other is transmitted toward the output polarizer H with a 100% efficiency in a perfectly aligned instrument with perfect polarizers. Furthermore, the two orthogonally polarized components of both the atmospheric and the reference signals have traveled different paths and when recombined through H will give rise to the desired interference. The principal axis of H is parallel or perpendicular to that of B. It is possible to verify that H gives one transmitted and one reflected output with 180° relative phase shift for both the atmospheric and reference signal. One output is the conventional interferogram with a positive signal relative to the dc level, and the other is the complementary interferogram with a negative signal relative to the dc level.

The two detectors, one at each output port, measure the interferogram given by the superimposition of the positive interferogram of one input and the negative interferogram of the other. The Fourier transform of such an interferogram supplies the difference between the spectral distribution of the atmospheric signal and the spectral distribution of the reference signal. The two detectors can cover the same spectral interval to increase the SNR after averaging or, as in our case, two different spectral intervals to extend the information over a wider spectral band without overloading the detectors beyond their photon noise limit.

A sketch of the instrument is shown in Fig. 2. The instrument is built in a modular arrangement of magnesium cast boxes. Magnesium was chosen to limit the weight despite the large dimensions of the instrument. The boxes can be made airtight to evacuate the instrument both for calibration purposes and in view of laboratory measurements.

B. Calibration

As described in Sec. III.A, the instrument measures a spectrum equal to the difference between the atmospheric signal and a reference signal reflected by the input polarizer. By means of a drive which locates the input polarizer in two different positions, it is possible

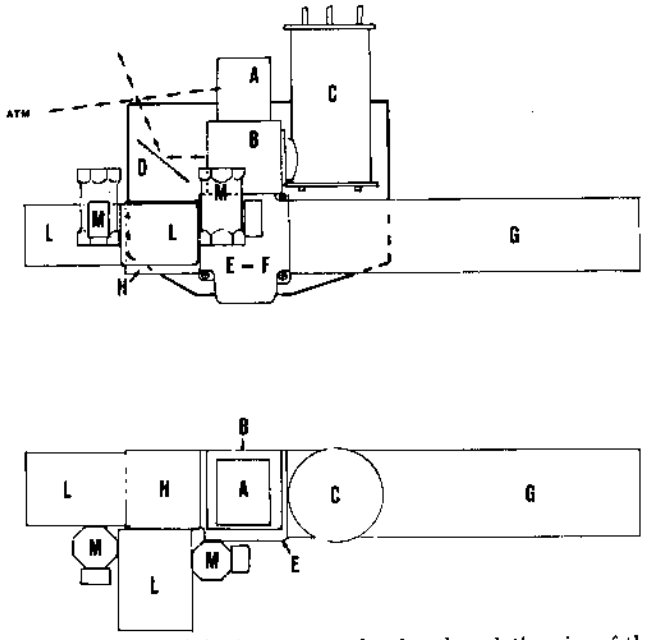

Fig. 2. Sketch of the instrument showing the relative size of the different components and the modular structure of the design. Note on the right the tall liquid nitrogen cryostat that cools the calibration blackbody source and the long arm with the moving mirror. On the left, the twin system of condensing optics and detector cryostat (letters as in Fig. 1).

to choose between two reference signals: the atmospheric zenithal emission (reflected by mirror D) and the emission from blackbody C at liquid nitrogen temperature (the blackbody is a larger version of the blackbody described in Ref. 21). The use of two reference sources provides a calibration simultaneous to the measurements as already done in the previous aircraft measurements.[6,17] Reference signals with emission comparable with the stratospheric emission have been chosen to limit the dynamic range of the signal and contain the effect of nonlinearities in the detector response.

C. Signal Modulation

One of the major choices was whether to modulate the radiation by means of an alternator and measure the signal by synchronous detection or operate in a rapid scanning mode.[22] The gain or loss in SNR corresponding to the different modes of operation of a spectrometer has been evaluated in Ref. 23. To this purpose, three parameters have to be considered: α, G_1, and G_2, where α, the signal coding efficiency, is a measurement of the losses introduced by the alternator; G_1 and G_2 are factors which measure the gain in SNR obtained when more than one detector and more than one output of the instrument are used. A relatively high value of the product $\alpha \cdot G_1 \cdot G_2$ (namely, 1) is obtained with a configuration which uses two detectors and an alternator operating between the two outputs of the spectrometer [$\alpha = 1/\sqrt{8}$ in the case of cosine modulation and real integration, $G_1 = \sqrt{2}$ and $G_2 = 2$; see Table I and Fig. 1(c) of Ref. 23]. This configuration can be easily put into practice in a polarizing interferometer by means of a polarizing alternator and has the interesting advantage of giving interferograms free from the dc level[1]; it requires, however, a very careful design to avoid spurious modulations due to nonplanarity of the alternator.

On the other hand, the product $\alpha \cdot G_1 \cdot G_2$ has an even higher value (equal to $\sqrt{2}$) in the case of a spectrometer used with a rapid scanning mode and real integration [$\alpha = 1$, $G_1 = 1$ and $G_2 = \sqrt{2}$, see Fig. 1(d) of Ref. 23].

A limitation of rapid scanning is that there is a reduced flexibility in the choice of the integration time and, therefore, in the obtainable SNR of the single interferogram due to the constraints in scanning speed set by the frequency response of the detecting system. Rapid scanning is not convenient whenever a poor SNR is obtained from a single scan, but the quality of present-day detectors (see Sec. VI) in association with the efficiency of polarizing beam splitters and the extra efficiency of rapid scanning itself makes possible in submillimeter wave measurements the reduction of the integration time to a point at which rapid scanning becomes usable and advantageous.

Considering also the need of recording the measurements in a short time when studying a variable source, the rapid scanning operation mode was adopted. The dc level subtraction which would have been obtained in an efficient way with the polarizing alternator was obtained by electrical filtering of the signal.

An interesting advantage resulting from the use of rapid scanning is that the signal may remain unaffected by accidental transients. In a case in point, the detection system was producing some additive transients due to burst from a leak in the cryostat. These transients did not affect the measurements since their frequency spectrum was outside the frequency range of the measured spectrum. In an instrument with an alternator, these transients would cause spikes which could only be corrected by manual editing. This type of advantage was pointed out in a similar instrument.[18]

IV. Sampling of the Signal

A. Signal Filtering

The choice of rapid scanning implies the use of a continuously and uniformly varying path difference (continuous movement of the mirror). The contents of this and of the following sections refer to this case.

The electric signal from the detector is always filtered to reduce the noise. Since an integration in the time domain corresponds to a filter in the frequency domain, resistance–capacitance (RC) and real integration are commonly used to this purpose for their simplicity. Other filters of both the analogic and digital types are in principle possible.

If $F(\nu)$ is the frequency response of the filter, both the noise and spectrum $S(\sigma)$ are attenuated by function $F(2v\sigma)$, where v is the speed of the moving mirror, and no change is experienced in SNR. However, when the signal is sampled at discrete points, folding occurs in the frequency domain, and the noise becomes larger being

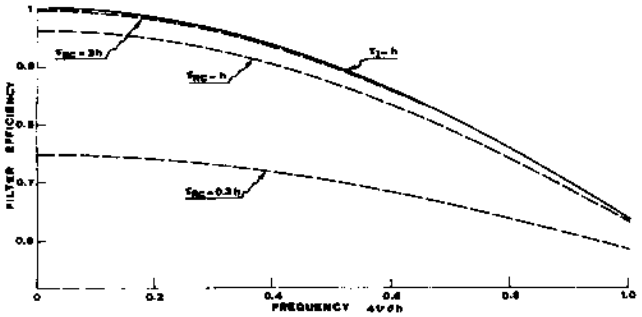

Fig. 3. Filter efficiency as a function of the frequency σ, normalized relatively to the Nyquist frequency $\sigma_N = (4\upsilon h)^{-1}$ in the case of RC integration (dashed lines) for three different values of the time constant τ_{RC} and in the case of real integration for a time τ_I (continuous line). Better efficiency is obtained for small values of σ relative to σ_N.

the result of the summation of the noise at several frequencies. As a consequence, a lower SNR is obtained with an efficiency which depends on the filter response.

The spectral distribution of the noise in the case of a discrete sampling and of RC and real integration has been calculated, e.g., by Connes.[24] In Ref. 23, the results of Connes have been used to evaluate the SNR efficiency corresponding to different integration functions and scanning methods. The expressions reported in Ref. 23 are calculated for the case of a measurement made with a phase error t_0. Taking σ for the wave number, υ for the speed of the moving mirror, and h for the sampling interval in the time domain, when a suitable phase error correction is introduced ($t_0 = -h/2$ for real integration and

$$t_0 = -\frac{\arctan 2\pi\upsilon\tau_{RC}}{2\pi\upsilon}$$

for RC integration), one finds that the SNR efficiency is equal to

$$E_{RC} = \left\{\frac{2\tau_{RC}[\cosh(h/\tau_{RC}) - \cos(4\pi\upsilon\sigma h)]}{h\sinh(h/\tau_{RC})[1 + (4\pi\upsilon\sigma\tau_{RC})^2]}\right\}^{1/2}. \quad (4)$$

in the case of RC integration with time constant τ_{RC} and to

$$E_I = \sqrt{\frac{\tau_I}{h}}\,\mathrm{sinc}(2\pi\upsilon\sigma h) \quad (5)$$

in the case of real integration for a time τ_I.

The function E_{RC} is plotted in Fig. 3 (dashed lines) as a function of $4\upsilon\sigma h$ for three different values of the ratio τ_{RC}/h. It turns out that higher values of E_{RC} are obtained with longer time constant τ_{RC} and in particular that

$$\lim_{\tau_{RC}/h\to\infty} E_{RC} = \mathrm{sinc}(2\pi\upsilon\sigma h). \quad (6)$$

This result is because a long integration time does not alter SNR at frequencies lower than the Nyquist frequency, since the same attenuation applies to both the signal and the noise and minimizes the effect of the noise which folds from frequencies higher than the Nyquist frequency. The advantage of a long integration time over a short one can be exploited only if the dynamic range of the electronics which processes the signal can cope with the attenuation that is introduced at high frequencies.

In the case of real integration, the highest value of E_I is obtained for $\tau_I = h$ and is equal to

$$E_I(\tau_I = h) = \mathrm{sinc}(2\pi\upsilon\sigma h). \quad (7)$$

The function $E_I(\tau_I = h)$ is also plotted in Fig. 3 (continuous line). While both types of integration give the same value of maximum efficiency, in spectra measured with real integration, the noise level is frequency independent so that no special requirement on the dynamic range of the electronics is involved. Also, real integration introduces a linear phase error in contrast with the nonlinear phase error of RC integration. On this basis real integration was adopted.

An improvement in the filtering efficiency can be obtained by choosing a higher Nyquist frequency (oversampling, see Sec. IV.C) so that the spectral region of interest (see Fig. 3) is less affected by noise folding.

B. Equal Time and Equal Space Sampling

Errors in the sampling position of the interferogram cause intensity errors in the spectrum. Useful treatments of this subject, which we have referred to for our evaluations, are described in Refs. 25 and 26.

Two sampling techniques with different effects in the intensity error of the spectrum can be used in the case of continuous mirror movement: equal time sampling and equal space sampling.

In the first case, the sampling position is accurately determined in the time domain and because of drive nonlinearities may occur in a position affected by an error $\delta x(t)$ in the space domain. In the second case, the sampling position is accurately determined in the space domain and because of drive nonlinearities may occur in a position affected by an error $\delta t(x)$ in the time domain.

In the case of equal time sampling and a random position error δx with a white spectrum and a standard deviation E, the root mean square intensity error $\langle\delta S(k\Delta\sigma)\rangle$ caused in the spectrum $S(k\Delta\sigma)$ by drive nonlinearities is equal to[25]

$$\langle\delta S^2(k\Delta\sigma)\rangle = (2\pi E)^2\frac{1}{n}\sum_{1^k}^{n}[k\Delta\sigma S(k\Delta\sigma)]^2. \quad (8)$$

Note that, when the power spectrum of the sampling error is different from zero at frequencies higher than the Nyquist frequency, oversampling (see Sec. IV.C) can be used to reduce the value of $\langle\delta S^2\rangle$.

In the case of equal space sampling, longer calculations are required for a rigorous evaluation of $\langle\delta S^2\rangle$ (see, e.g., Ref. 26). As it is outside the aim of this paper to analyze the general problem, we shall limit ourselves to some qualitative considerations.

With equal space sampling no error is made by definition in the sampling position, but because of the frequency-dependent delay $t_d(\sigma)$ introduced by the time constant of the detector and by the signal filtering, the signal measured at time t is the signal which reached the detector at time $t - t_d(\sigma)$ (note the dependence on the

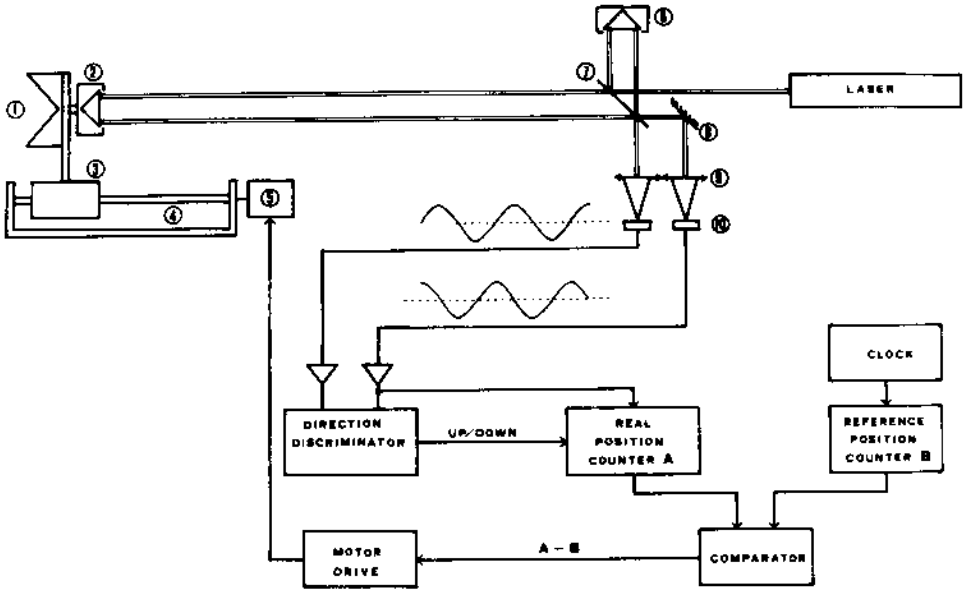

Fig. 4. Block diagram of the mirror movement control: (1) roof mirror; (2) cube corner mirror; (3) carriage; (4) lead screw; (5) motor; (6) fixed cube corner mirror; (7) beam splitter; (8) mirror; (9) lens; and (10) photoconductor.

frequency). This delay can be compensated only partially by postponing the sampling instant by a suitable constant time t_x. The residual error depends on the correlation existing between the position error $\delta x(t)$ and the position error $\delta x(t - t_d + t_x)$. This correlation can be increased by damping the high-frequency components for the mirror driving system (at the expense of the increase of the low-frequency error) and/or by minimizing the value of $t_d - t_x$ as a function of frequency, that is, by reducing the phase nonlinearity in the signal measurement system.

Phase nonlinearity can either be avoided by using fast detectors and filters with a linear phase or be compensated for by correcting for the phase error before sampling. In the case of submillimeter measurements from a balloon-borne platform, both solutions appear to have some limitations. First, the detectors are of the bolometric type, and best performances are achieved with long time constants; second, the reliability of a remotely controlled experiment may be recommended to minimize the onboard data processing.

In general, a better accuracy is obtained with equal space sampling because a more precise correction can be applied electronically in the time domain than mechanically in the space domain. For this reason, equal space sampling is adopted in most FT spectrometers operating at short wavelengths. On the other hand, at long wavelengths the precision required in the mirror movement can be achieved with conventional control systems (see Sec. V). In these conditions the method of equal time sampling was preferred because of its simplicity and reliability. In particular, the method does not require a time normalization in the case of real integration measurement (see Sec. IV.A) and makes simple the synchronization with the data acquisition system.

C. Oversampling

If the spectral distribution is different from zero in the interval $0 - \sigma_{max}$, to avoid overlapping of different spectral regions due to the folding of the frequency domain, the sampling interval h must be shorter than $1/2\sigma_{max}$. As pointed out in previous sections, the use of a sampling interval appreciably shorter than the limit $1/2\sigma_{max}$ (oversampling) can help to minimize the effects due to the folding of both noise and sampling errors. These advantages are achieved at the expense of a larger data flow. In our case, since the instrument was used on a balloon-borne gondola with a limited bit rate in the telemetry system, oversampling was not possible. The sampling interval was made equal to 25 μm (corresponding to a path difference $\Delta x = 50$ μm) equivalent to a Nyquist frequency of 100 cm^{-1}. Some flexibility was left in the instrument to make possible the change of the sampling interval in different applications.

V. Movement Control

A block diagram of the movement control system is shown in Fig. 4. The position of a cube corner mirror simultaneously moving rigidly with the moving mirror of the spectrometer is measured by means of interferometric measurements with a laser source.[27] The laser is a single-mode single-frequency laser model 100 Tropel with a coherence length much longer than the mirror movement. The cube corner retroreflectors abate the alignment precision requirements for the laser interferometer and make it possible to separate the second output from the input beam. Both outputs of the interferometer are monitored, and a special beam splitter[28] is used to produce a phase difference of +90° between the two outputs depending on the direction of the movement. This direction indicator is used together

with the interference train to drive a counter which measures the mirror position. The real position given by this counter is continuously compared with the nominal position given by a reference counter, and the difference is used in a closed-loop feedback to control the mirror drive. The real position counter can be sampled together with the spectrometer signal. This information was used to calculate the error of the mirror position $dx = \frac{1}{2}\delta x(t)$. The histogram of the distribution of dx is shown in Fig. 5, where it is compared with a Gaussian distribution with a variance of 0.33 μm, equivalent to a path difference error $E = 0.66$ μm.

As suggested by the Gaussian distribution, the position error is dominated by a component of white noise. Assuming that the measured spectrum is made of m lines ($m < n$) of intensity I uniformly distributed throughout the spectral interval from 0 to 100 cm^{-1}, we obtain from Eq. (8)

$$\frac{I}{\langle \delta S^2 \rangle} = \frac{1}{2\pi E \sigma_{\max}} \sqrt{\frac{3n}{m}}. \tag{9}$$

In our case, the position error sets an upper limit to the SNR of the spectrum equal to

$$\mathrm{SNR} \leq 50 \sqrt{\frac{n}{m}}. \tag{10}$$

Since n is always at least 1 order of magnitude $> m$, this error is not the limiting factor in the final SNR (see Sec. VIII).

VI. Detecting System

Figure 6 shows a diagram of the condensing optics. The output beam from the interferometer is focused by an off-axis paraboloid; a flat mirror folds the converging beam reducing the volume of the system. Catoptric optics was chosen to avoid absorption losses in lens material at high frequencies. An off-axis parabolic mirror was preferred to either a Cassegrain system or a spherical condenser because of losses due to shadowing in the first case and to aberration in the second. The radiation is focused through a thin Mylar window on the cooled optics of the detector composed of a cone and a coupling TPX lens which matches the angular response of the cone to the distribution of the illumination on the paraboloid.[29] A cold filter that limits the radiation load on the detector and a cold limiting aperture that defines the solid angle of the beam (see Sec. II) are located next to the lens.

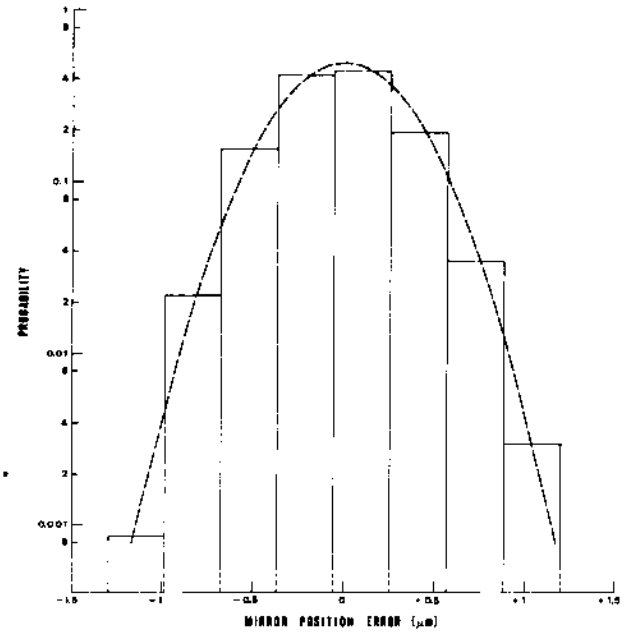

Fig. 5. Histogram of the mirror position error fitted by a Gaussian distribution.

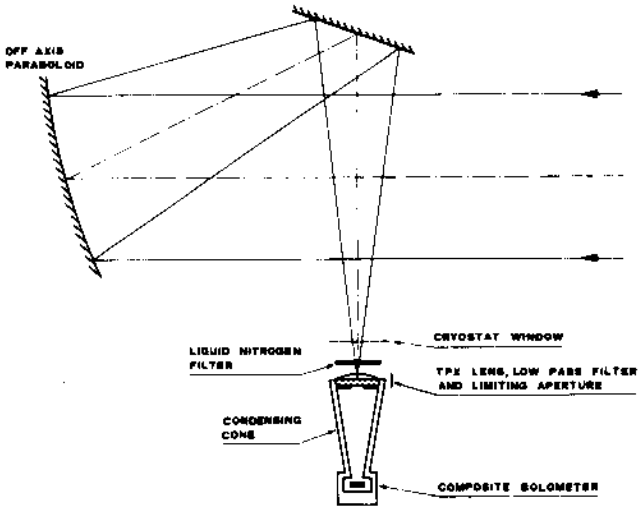

Fig. 6. Diagram of the condensing and detector optics.

The detectors are composite germanium bolometers. Some of the bolometers were provided by Queen Mary College (London, U.K.),[30] and others were made by Infrared Laboratories (Tucson, Ariz.). The noise equivalent power (NEP) of a bolometer can be optimized to respond to a desired modulation frequency ν with a suitable choice of the time constant of the bolometer (see, e.g., Ref. 31). In a rapid scanning interferometer, where the signal at each wave number σ is modulated at a different electrical frequency $\nu = 2v\sigma$, a broad band of modulation frequencies exists, and optimization can only be partial.

The low-frequency interval (7–45 cm^{-1}) was covered by a detector with a relatively long time constant ($\tau_1 =$ 6 msec), while the high-frequency interval (30–90 cm^{-1}) was covered by a faster detector ($\tau_2 = 2$ msec). As a consequence of the different time constant, the low-frequency detector has a lower NEP (1.4×10^{-14} W/$\sqrt{\mathrm{Hz}}$) than the high-frequency detector (4.6×10^{-14} W/$\sqrt{\mathrm{Hz}}$).

The experimental spectral responsivity of the two detectors, which includes losses introduced by window, lens, and filters, interferometer efficiency, and frequency response both of the detectors and of signal integration (see Sec. IV.A), is shown in Fig. 7 together with the noise spectra measured during the balloon-borne operation.

The periodic variation which is present in the responsivity is due to optical interference within the thickness of some of the dielectric materials encountered by the beam.

The noise is substantially higher than the intrinsic detector noise and is caused mainly by some microphonics (note the presence in both detectors of a peak of noise $\sim 20\ cm^{-1}$) and by digitization noise in the ADC as a result of an inefficient dynamic range in the signal electronics (the difference of a factor of ~ 2 in the noise of the two detectors is related to the different gain in the preamplifiers).

Despite the imperfect performances of the bolometers, spectra with a useful SNR have been obtained, and significant new information has been acquired on the stratospheric emission spectrum (see Sec. VIII.D).

VII. Data Analysis

A. Phase Error Corrections

The measurements are taken on one side of the zero path difference point (single-sided interferogram). A few measurements are recorded each time on the other side to get a short double-sided interferogram which provides information on the phase at low resolution. In this way the available mirror displacement is fully exploited to maximize the spectral resolution, but an elaborate procedure must be used to correct for phase errors.

Sources of phase error are

(1) Zero path difference error. This error is due to a shift of the sampling points comb relative to the ideal pattern, where one sampling point coincides with the zero path difference position. The resulting phase error is linear: $\phi_1 = \pi\varepsilon\sigma$.

(2) Time response of the bolometer. This error is caused by time constant τ of the bolometer and can be represented as the delay of an RC integration: $\phi_2 = \arctan(2\pi\tau \cdot 2v\sigma)$, where v is the speed of the moving mirror.

(3) Electronic integration. The integration of the electric signal from the bolometer also causes a phase delay which depends on the type of integration. For RC integration with the time constant τ_{RC}, $\phi_3 = \arctan(2\pi\tau_{RC} \cdot 2v\sigma)$. For real integration, as in the present case, $\phi_3 = 2\pi\tau_I\sigma$, where τ_I is the integration time.

(4) Misalignment. Misalignment in the optics of the interferometer can cause phase errors. A quantitative evaluation of this type of error in the case of a polarizing interferometer has been made in Ref. 32.

(5) Optical components which introduce a frequency-dependent phase delay.

In our measurements, the last two sources are negligible, and the phase error is well represented by the analytical expression

$$\phi(\sigma) = 2\pi\sigma(\varepsilon + v\tau_I/2) + \arctan(4\pi\tau v\sigma). \qquad (11)$$

The phase correction method by Forman *et al.*,[33] which also corrects nonlinear errors, has been used. According to this method, the phase function $\phi(\sigma)$ is calculated from a short double-sided interferogram and is used to correct the high-resolution single-sided interferogram. This method gave satisfactory results in the majority of cases but turned out to be inadequate in the case of spectra where a change of sign is present.

The cause of this problem is twofold. First, a change of sign is equivalent to a phase error of π, so that a conventional phase error procedure changes the sign of the spectrum wherever it detects a negative signal. Second, the low-resolution spectrum, which is used to measure the phase error, usually displays a very low SNR in the frequency interval where the change of sign takes place. As a consequence, a large error can be made in the measurement of the phase at those frequencies.

Changes of sign occur frequently in the measurement of atmospheric emission against the emission of the blackbody at liquid nitrogen temperature as the first is higher than the second at frequencies where saturated emission lines are present and lower at frequencies where the atmosphere is transparent. An *ad hoc* procedure based on Eq. (11) was developed to correct the phase error of these spectra and provided satisfactory results.[34]

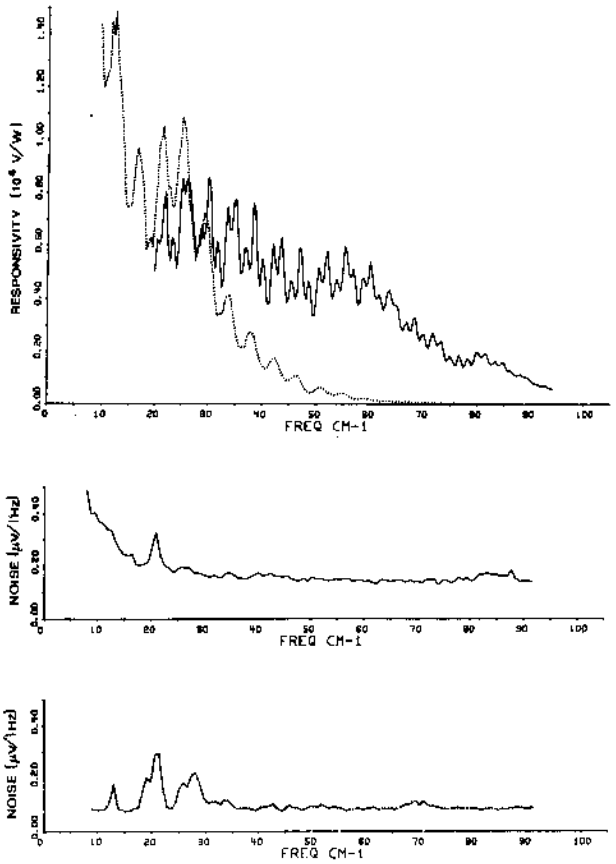

Fig. 7. Responsivity and noise as a function of wave number for the low-frequency detector (dotted line) and the high-frequency detector (continuous line).

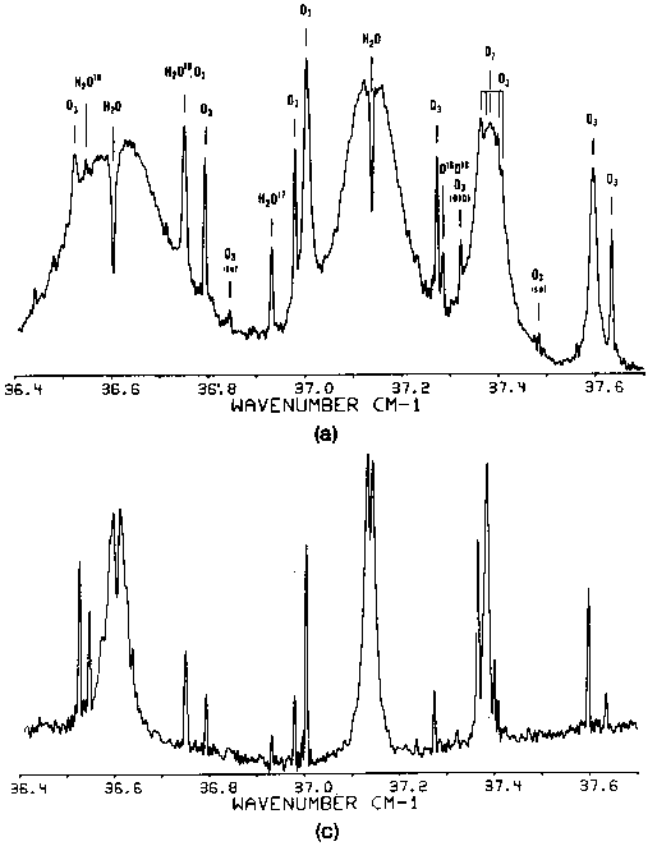

Fig. 8. Atmospheric emission measured from ~40-km altitude with a resolution of 0.0033 cm^{-1}. The unapodized spectrum with one interpolation point is shown for three different limb scan angles: 3.6, 1.6, and 0° below the horizontal direction in (a), (b), and (c), respectively. The vibrational state is indicated in parentheses in the case of vibrationally excited transitions. The label O_3 isot. indicates transitions due to $O^{16}O^{18}O^{16}$. The negative dip in the center of the strong water vapor line is due to absorption within the instrument.

B. Spectral Interpolation

The sampling theorem (see, e.g., Ref. 35) states that, from a single-sided interferogram of n data points, it is not possible to retrieve more than n independent measurements in the frequency domain. Nevertheless, the graphical presentation of the spectrum is visually more descriptive when extra points are introduced between the independent measurements. This interpolation can be made either in the space domain by extending the interferogram with zero filling[36] or in the frequency domain by convolution.[37] Reference 38 gives a comparison of the number of computer operations required by each method.

In our measurements, different spectra and, in particular, different spectral regions often require a different apodization (see Sec. VII.C) and a different number of interpolation points. For this reason it was decided to make both the interpolation and the apodization with the convolution method so that different presentations of the spectrum are obtained without reprocessing the interferogram each time.

The spectra shown in this paper are plotted with one intermediate point which corresponds to a factor of 2 zero filling.

C. Apodization

The instrumental function of an FT instrument is equal to $\mathrm{sinc}(2\pi\sigma D)$, where D is the maximum path difference. The secondary maxima of this function can cause false features, and it is common practice to use an apodization of the interferogram to modify the instrumental function and reduce the amplitude of these maxima (for a general treatment, see Ref. 39). This result is achieved at the expense of the width of the instrumental function and of the resolution.

In the case of atmospheric emission spectra at high resolution, three cases are possible: (a) emission spectra from atmospheric layers at relatively high pressure ($P > 30$ mbar), where the line profiles are dominated by the pressure broadening and the secondary maxima of the instrumental function do not distort the spectrum [see Fig. 8(a)]; (b) emission spectra from layers at intermediate pressure (30 mbar $> P >$ 5 mbar), where both the lines are not resolved and a high SNR is obtained. In this case [see, for example, the O_3 line at 36.8 cm^{-1}, Fig. 8(b)] the instrumental function determines the shape of the lines and the secondary maxima become visible. (c) Emission spectra from layers at low pressure ($P < 5$ mbar), where the halfwidth of the lines is much less than the instrumental resolution. This means that the SNR of most lines is low, and it is not possible to identify the weak secondary maxima against the relatively high noise [see Fig. 8(c)].

Only in a few isolated cases of saturated lines (see, for example, the O_3 line at 37.0 cm^{-1}) is the signal large enough to see the secondary maxima of the instrumental function. Furthermore, in the few cases for which apodization would have been convenient, comparison with the corresponding spectra at high pressure removes most of the ambiguities. In our analysis, apodization was not used to keep the resolution at its highest value.

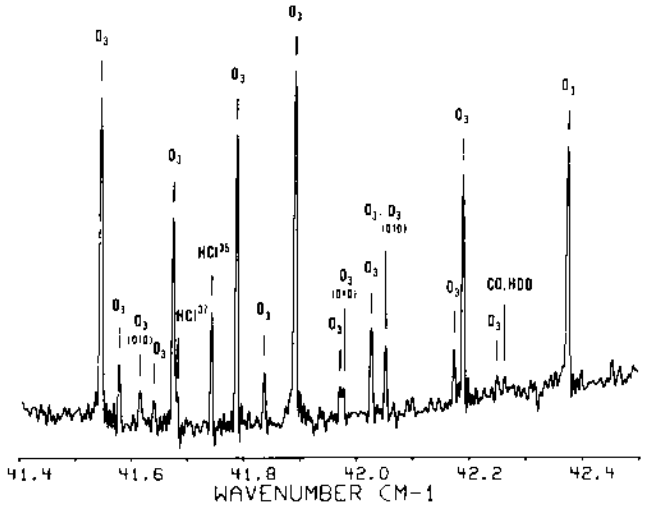

Fig. 9. Sample of an atmospheric emission spectrum from ~40-km altitude looking in the horizontal direction. The unapodized spectrum makes it possible to resolve the two features of ozone at ~41.97 cm^{-1} that are 5.5×10^{-3} cm^{-1} apart.

VIII. Final Remarks

A. Resolution

The maximum path difference of 150 cm (see Sec. II) provides independent information on the spectral frequency domain with a period of 0.0033 cm^{-1}. The spectroscopic resolution of the measurement intended as the minimum distance between two resolved features depends also on other factors such as solid angle and SNR. A measurement of this minimum distance is rather difficult as it requires the occurrence of several coincidences. The lines must have almost equal intensity, the right frequency separation, and both a large enough integral intensity to be measurable above the noise level and a small enough halfwidth to be considered as delta functions.

Figure 9 shows the case of two lines which approach these constraints. The first is a line due to ozone in the ground state at 41.9721 cm^{-1}, and the second is a line due to ozone excited to the first ν_2 level at 41.9776 cm^{-1}. These lines are clearly resolved, and their separation of 5.5×10^{-3} cm^{-1} is very close to the value of 4.8×10^{-3} cm^{-1}, the limit of resolution following the Rayleigh criterion in the case of our sinc instrumental function. This example corresponds to a resolving power of ~8000, that is, of the order of the maximum resolving power of 12,000 made possible by the solid angle of the beam.

A second example of closely resolved lines is the case of the HCl^{37} transition at 41.6813 cm^{-1} that is present in Fig. 9 as a shoulder to the ozone transition at 41.6751 cm^{-1}.

B. Signal-to-Noise Ratio

In the case of a single stratospheric emission spectrum recorded in 4 min, the SNR in each spectral element, 0.0033 cm^{-1} wide, varied from 20 to 40 depending on the detector and on the frequency. A limit to the value of SNR was set by microphonics and digitization noise (see Sec. VI), which turned out to be higher than the detector noise. The noise caused by position errors can be considered to be negligible relative to the others (see Sec. V). All sources of noise are uncorrelated from one spectrum to another, thus when averaging measurements of the same source, an improvement in SNR proportional to the square root of the number of spectra is to be expected. This has been verified in the limits of the available data on averages of up to eight spectra.

C. Frequency Accuracy

A frequency accuracy better than 2×10^{-4} cm^{-1} in the central position of isolated lines is obtained throughout the full spectral interval.[40] While a less precise value is obtained when nearby features distort the line as often happens in stratospheric spectra, the accuracy is still good enough to provide substantial evidence for the assignment of the observed features.[41]

D. Outline of Results

The instrument was successfully used for stratospheric emission measurements from a balloon-borne platform at ~40-km altitude. The high resolution made it possible to detect in the atmospheric spectrum, superimposed on the dominant structure of the ozone, oxygen, and water vapor spectrum, several rotational lines due to minor constituents such as HF, HCl^{35}, HCl^{37}, HCN, CO, OH, N_2O, NO, and HNO_3. Several other new features have been assigned to isotopic species and vibrationally excited molecules, namely, $O^{16}O^{18}O^{16}$,$O^{16}O^{16}O^{18}$, ozone excited to the ν_1, ν_2, and ν_3 first vibrational level, $O^{16}O^{18}$, H_2O^{18}, H_2O^{17}, HDO, and water vapor excited to the first ν_2 level.[8-10]

This work was financially supported by the Space Research Commission, by the Committee for Physical Sciences of the Italian National Research Council, and by the Chemical Manufacturers Association (contract FC-76/137). We wish to record our gratitude to Francesco Scandone for his personal interest and his generous support.

One of us (B.C.) is indebted to D. H. Martin for his scholarly critical guide into the subject of far-infrared Fourier transform spectroscopy.

The instrument was built thanks to the skill and dedication of several experts and specialized firms: E. F. Puplett designed the mirror mounts, A. E. Costley provided the free-standing-wire polarizers, S. El-Atawy manufactured some of the bolometers, K. W. Raine provided the coating of the beam splitter for the laser interferometer, D. Pucci manufactured the optical components for the laser interferometer, M. Cellini made the mechanical drawings, the firm Marcon of San Donà di Piave manufactured the off-axis paraboloids, Campagnolo of Bologna made the magnesium castings, Salvadori of Firenze machined and assembled the instrument, and Microdata of Lerici designed and constructed the electronics.

We acknowledge with pleasure the support of

IROE-CNR and the University of Florence: G. Toraldo di Francia, F. Melchiorri, V. Natale, and S. Aiello. G. Ventura gave valuable help in the limb-scan electronics. M. G. Baldecchi, F. Castagnoli, and I. Pippi were of assistance during the assembling and testing of the instrument. E. Rossi contributed to the success of the experiment during both the laboratory work and the field operation.

The stratosphere measurements were performed from the National Scientific Balloon Facility, Palestine, Tex. in the frame of the NASA-LIMS project in a collaboration with the National Physical Laboratory, Teddington, U.K. It is a pleasure to recall the cooperation of J. H. Harries and the colleagues of NPL Quantum Metrology Division, in particular R. Bradsell. We acknowledge with gratitude the help received from I. Nolt and J. Radostitz of the University of Oregon.

References

1. D. H. Martin and E. F. Puplett, "Polarized Interferometric Spectrometry for the Millimeter and Submillimeter Spectrum," Infrared Phys. **10**, 105 (1970).
2. E. I. Robson, D. G. Vickers, J. S. Huizinga, J. E. Beckman, and P. E. Clegg, "Spectrum of the Cosmic Background Radiation between 3 mm and 800 μm," Nature (London) **251**, 591 (1974).
3. D. P. Woody, J. P. Mather, N. S. Nishioka, and P. L. Richards, "Measurement of the Spectrum of the Submillimeter Cosmic Background," Phys. Rev. Lett. **34**, 1036 (1975).
4. B. Carli *et al.*, "Preliminary Results of Measurements of Atmospheric Emission and Absorption at Infrared Wavelengths at Gornergrat," Mem. Soc. Astron. Ital. **47**, 101 (1976).
5. R. E. Hills *et al.*, "Absolute Measurements of Atmospheric Emission and Absorption in the Range 100–1000 GHz," Infrared Phys. **18**, 819 (1978).
6. B. Carli, D. H. Martin, E. F. Puplett, and J. E. Harries, "Measurements of Ozone and Minor Atmospheric Constituents," Nature (London) **257**, 649 (1975).
7. A. Bonetti, B. Carli, F. Mencaraglia, J. E. Harries, M. J. Bangham, and D. H. Martin, *Atmospheric Physics from Spacelab*, J. J. Burger *et al.*, Eds (Reidel, Dordrecht, 1976), pp. 329–338.
8. B. Carli, F. Mencaraglia, and A. Bonetti, "Fourier Spectroscopy of the Stratospheric Emission," Int. J. Infrared Millimeter Waves **1**, 263 (1980).
9. B. Carli, F. Mencaraglia, and A. Bonetti, "New Assignments in the Submillimeter Spectrum of the Stratosphere," Int. J. Infrared Millimeter Waves **3**, 385 (1982).
10. B. Carli, F. Mencaraglia, A. Bonetti, B. M. Dinelli, and F. Forni, "Submillimeter Detection of Stratospheric OH and Further Line Assignments in the Stratospheric Emission Spectrum," Int. J. Infrared Millimeter Waves **4**, 475 (1983).
11. H. A. Gebbie, W. J. Burroughs, J. E. Harries, and R. H. Cameron, "Submillimeter Wave Spectroscopy of the Earth's Atmosphere Above 39000 Feet," Astrophys. J. **154**, 405 (1969).
12. J. A. Eddy, R. H. Lee, P. J. Lena, and R. M. MacQueen, "Far Infrared Airborne Spectroscopy," Appl. Opt. **9**, 439 (1970).
13. J. E. Harries and W. J. Burroughs, in *Proceedings Infrared Techniques Conference, Reading* (IERE, London, 1971), p. 271.
14. I. G. Nolt, J. V. Radostitz, and R. J. Donally, "Upper Atmosphere Emission Spectrum at Millimeter Wavelengths," Nature (London) **236**, 445 (1972).
15. J. E. Harries, N. R. W. Swann, G. P. Carruthers, and G. A. Robinson, "Measurement of the Submillimetre Stratospheric Spectrum from a Balloon Platform," Infrared Phys. **13**, 149 (1973).
16. J. P. Baluteau, E. Bussoletti, A. Langlet, and J. Roucher, "Détermination de Spectres d'Emission Du Ciel Dans l'Infrarouge Entre 45 et 500 μm à Partir d'un Interféromètre Embarqué en avion," ESRO/ELDO Sci. Tech. Rev. **4**, 353 (1972).
17. B. Carli, D. H. Martin, E. F. Puplett, and J. E. Harries, "Very-High-Resolution Far-Infrared Measurements of Atmospheric Emission from Aircraft," J. Opt. Soc. Am. **67**, 917 (1977).
18. D. J. W. Kendall and T. A. Clark, "Balloon-borne Far Infrared Michelson Interferometer for Atmospheric Emission Studies," Appl. Opt. **18**, 346 (1978).
19. P. Jacquinot, "New Developments in Interference Spectroscopy," Rep. Prog. Phys. **23**, 268 (1960).
20. A. E. Costley, K. H. Hursey, G. F. Neill, and J. W. Ward, "Free-standing Fine-Wire Grids: Their Manufacture, Performance, and Use at Millimeter and Submillimeter Wavelengths," J. Opt. Soc. Am. **67**, 979 (1977).
21. B. Carli, "Design of a Black Body Reference Standard for the Submillimeter Region," IEEE Trans. Microwave Theory Tech. **MTT-22**, 1904 (1974).
22. L. Mertz, *Transformation in Optics* (Wiley, New York, 1966).
23. B. Carli and V. Natale, "Efficiency of Spectrometers," Appl. Opt. **18**, 3954 (1979).
24. J. Connes, "Recherches sur la Spectroscopie par Transformation de Fourier," Rev. Opt. **40**, 171 (1961).
25. E. E. Bell and R. B. Sanderson, "Spectral Errors Resulting from Random Sampling-Position Errors in Fourier Transform Spectroscopy," Appl. Opt. **11**, 688 (1972).
26. A. S. Zachor, "Drive Nonlinearities: Their Effects in Fourier Spectroscopy," Appl. Opt. **16**, 1412 (1977).
27. W. R. C. Rowley, "Bidirectional Counting for the Measurements of Laser Beat Frequencies," J. Phys. E. **8**, 223 (1975).
28. K. W. Raine and M. J. Downs, "Beam Splitter Coatings for Producing Phase Quadrature Interferometer Outputs," Opt. Acta **25**, 549 (1978).
29. W. L. Wolfe, *Handbook of Military Infrared Technology* (Office of Naval Research, Washington, D.C., 1965).
30. S. El-Atawy, P. A. R. Ade, J. V. Radostitz, and I. G. Nolt, "Evaluation of Composite Bolometers at 0.4 Kelvin," Int. J. Infrared Millimeter Waves **1**, 459 (1980).
31. N. Coron, "A New Type of Helium-Cooled Bolometer," Infrared Phys. **16**, 441 (1979).
32. D. K. Lambert and P. L. Richards, "Martin-Puplett Interferometer: an Analysis," Appl. Opt. **17**, 1595 (1978).
33. M. L. Forman, W. H. Steel, and G. A. Vanasse, "Correction of Asymmetric Interferograms Obtained in Fourier Spectroscopy," J. Opt. Soc. Am., **56**, 59 (1966).
34. B. Carli, F. Forni, and F. Mencaraglia, "Phase Error Correction in FT Spectroscopy of Spectra with Positive and Negative Intensities," Int. J. Infrared Millimeter Waves **3**, 529 (1982).
35. C. Shannon, "Communication in the Presence of Noise," Proc. IRE **37**, 10 (1949).
36. B. Gold and C. Rader, *Digital Processing of Signals* (McGraw-Hill, New York, 1969).
37. J. Connes, ASPEN International Conference on Fourier Transform Spectroscopy, AFCRL-71-0019, S.R. 114, 83 (1970).
38. M. L. Forman, "Spectral Interpolation: Zero Fill or Convolution," Appl. Opt. **16**, 2801 (1977).
39. F. J. Harris, "On the Use of Windows for Armonic Analysis with Discrete Fourier Transform," Proc. IEEE **66**, 51 (1978).
40. M. G. Baldecchi, B. Carli, M. Carlotti, G. Di Lonardo, F. Forni, F. Mencaraglia, and A. Trombetti, "High Resolution Molecular Spectroscopy in the Submillimeter Region," J. Infrared Millimeter Waves **5**, 281 (1984).
41. M. G. Baldecchi, A. Bonetti, B. Carli, M. Carlotti, and F. Mencaraglia, "Atlas of Stratospheric Submillimeter Lines—1. The 7–20 cm^{-1} Interval," J. Geophys. Res. (1984).